Chapter 5

Impact of 13-93 bioactive glass addition on the structural, mechanical, *in-vitro* degradation, cell culture, and antibacterial response of the Mg-PSZ-based biocomposite materials

5. 1 Introduction

Nowadays, humans suffering from accidents and joint diseases, such as different types of arthritis, osteoporosis, and dental restorations, may undergo surgical implants. For the last few decades, ZrO_2-based bioceramic composites have been used as load-bearing materials for total hip arthroplasty because fatal failure occurs in Al_2O_3 femoral heads during *in-vivo* applications (Rahaman *et al.*, 2007) (Ghalme *et al.*, 2016). The three mole% yttria-stabilized zirconia (3Y-TZP) ceramic has better mechanical properties than Al_2O_3 (Rahaman *et al.*, 2007). However, 3Y-TZP ceramic undergoes transformation, and deterioration occurs at autoclaving temperatures during steam sterilization (Chevalier *et al.*, 2007). The 3Y-TZP femoral heads were eliminated from orthopedics use in 2001 due to the high incidence of *in-vivo* failure (Masonis *et al.*, 2004).

ZrO_2 is partially stabilized with magnesium oxide (MgO), known as Mg-PSZ. Compared to 3Y-TZP, Mg-PSZ exhibits favorable characteristics, including good mechanical and thermal properties, low-temperature deterioration stability, and the same thermal expansion coefficient (TEC) as 3Y-TZP (Yusuf *et al.*, 2023). The pure Mg-PSZ is bio-inert ceramic (Dehestani *et al.*, 2012). Its application as a femoral-bearing implant necessitates the use of bone cement. There are many problems with bone cement, such as the possibility of cement disintegration and degradation, leading to periprosthetic swelling, increasing bone erosion, and eventual implant instability (Rahaman *et al.*, 2008). As a result, removing bone cement while achieving long-lasting implant-bone bonding is preferable.

The addition of BG into pure ZrO_2 ceramics imparts bioactivity and forms a strong bond with host tissue when it is implanted in the human body (Ho *et al.*, 2011) (Habibe *et al.*, 2009) (de Paula *et al.*, 2019). Another advantage of the BG addition into ZrO_2 ceramics is to improve the densification at lower sintering temperatures (Bicalho *et al.*, 2011). In addition to these advantages of BG incorporation, many researchers have reported that the combined

additions of Ca^{2+}, PO_4^{-3}, and SiO_2 act as aging resistance and restrict the transformation from t-ZrO_2 to m-ZrO_2 (Vasanthavel *et al.*, 2016) (Del Monte *et al.*, 2000).

The intent of the research work is to synthesize an 8Mg-PSZ-based bioactive glass composite. Sample code and different compositions of 8Mg-PSZ/13-93 BG biocomposite materials are given in Table 3.2. In this chapter, the effect of 13-93 BG additions on the structural, mechanical, *in-vitro* degradation, cell culture, and antibacterial response of 8Mg-PSZ-based bioceramic composite materials are evaluated.

5.2 Results and discussion

5.2.1 Particle size, XRD, SEM, and FTIR analysis of the prepared precursor

DLS is used to analyze the distribution of particle sizes of the synthesized powders by volume. DLS employs a standard spherical particle type with a scattering angle of 90º. The 8Mg-PSZ powders are dispersed in acetone and put under a probe sonicator to form an aqueous solution. The average particle size of the 8Mg-PSZ is around 855±89 nm, as shown in Fig. 5.1(a). The majority of the tetragonal phase of ZrO_2 (t-ZrO_2), reference code (98-002-7991), is found in the XRD pattern of prepared 8Mg-PSZ powders, as represented in Fig. 5.1(b)**.** Fig. 5.1(c) displays the SEM images of the synthetic matrix (8Mg-PSZ ceramic). The 8Mg-PSZ powder shows tiny powder particles with little agglomeration. The FTIR spectroscopy of the calcined 8Mg-PSZ ceramic powder was studied in the region of 550 – 4000 cm^{-1}, as shown in Fig. 5.1(d). The major characteristic bands are located at 590, 940, 1414, 1480, 2363, 2961 and 3429 cm^{-1}. The characteristic transmittance bands for Zr–O bonds appear at 590 cm^{-1} (Yadav *et al.*, 2021), and 940 cm^{-1} corresponds to Mg-O bonds (Wahyudi *et al.*, 2021). These zirconium oxygen bonds indicate the existence of ZrO_2 in the synthesized samples.

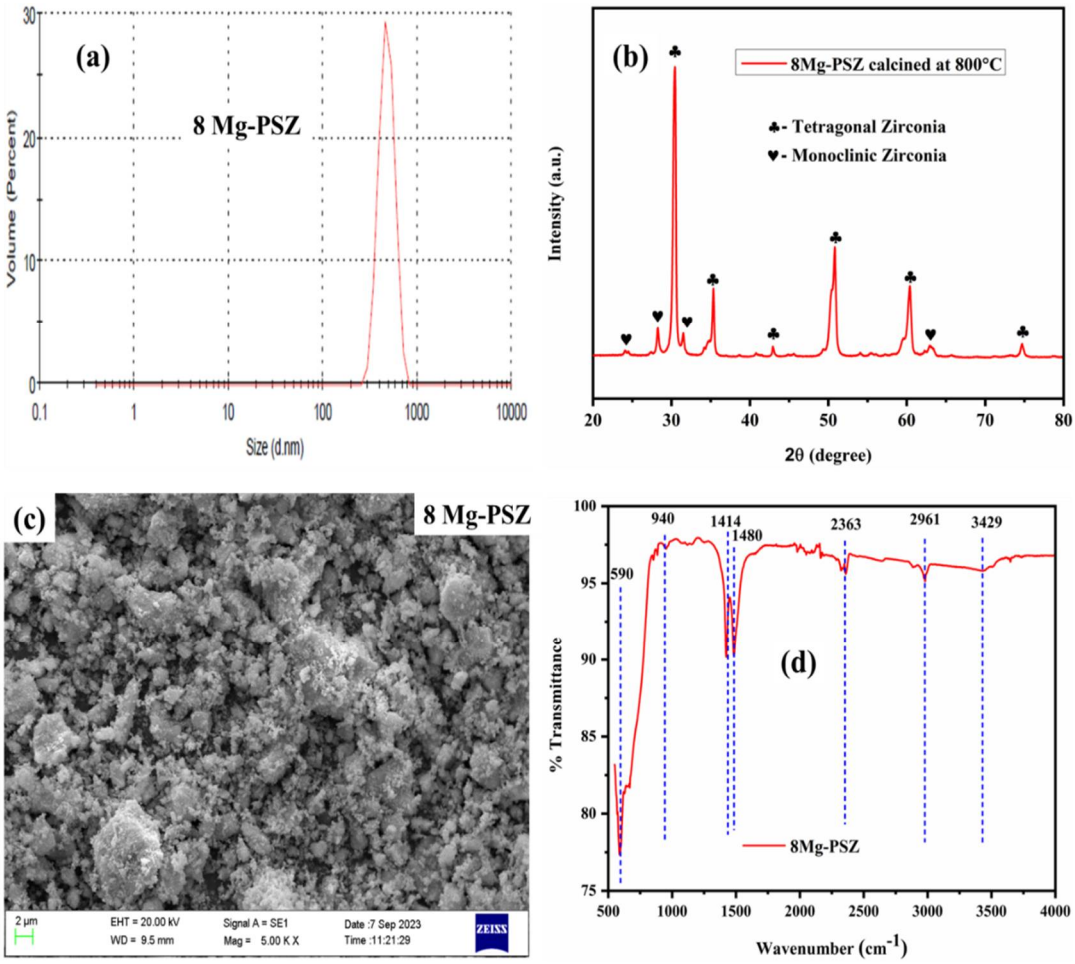

Fig. 5.1 Characterization of prepared 8Mg-PSZ powder (a) Particle size measurement (b) XRD analysis (c) SEM, and (d) FTIR spectra.

The characteristic bands located at 1414 and 1480 cm^{-1} are caused by the adsorbed CO_2 from the air (Qiu *et al.*, 2022) (Chen *et al.*, 2021). The characteristic bands located at 2363 and 2961 cm^{-1} are formed by the -C-H bonds (Habibe *et al.*, 2009). The entire process is performed in deionized water, as a result of which a strong Zr–OH transmittance band appears at 3429 cm^{-1} (Qiu *et al.*, 2022) (Chen *et al.*, 2021). The XRD spectra of the pure 8Mg-PSZ powder calcined at various temperatures, between 600°C to 1350°C, are displayed in Fig. 5.2. At 600°C, the 8Mg-PSZ powder remains in the tetragonal phase. The tetragonal phase is seen to be retained up to 900°C. There is a noticeable phase transition between pure t-ZrO_2 and pure m-ZrO_2 between 1000 and 1350°C. The characterization of BG is explained in Section 4.2.1.

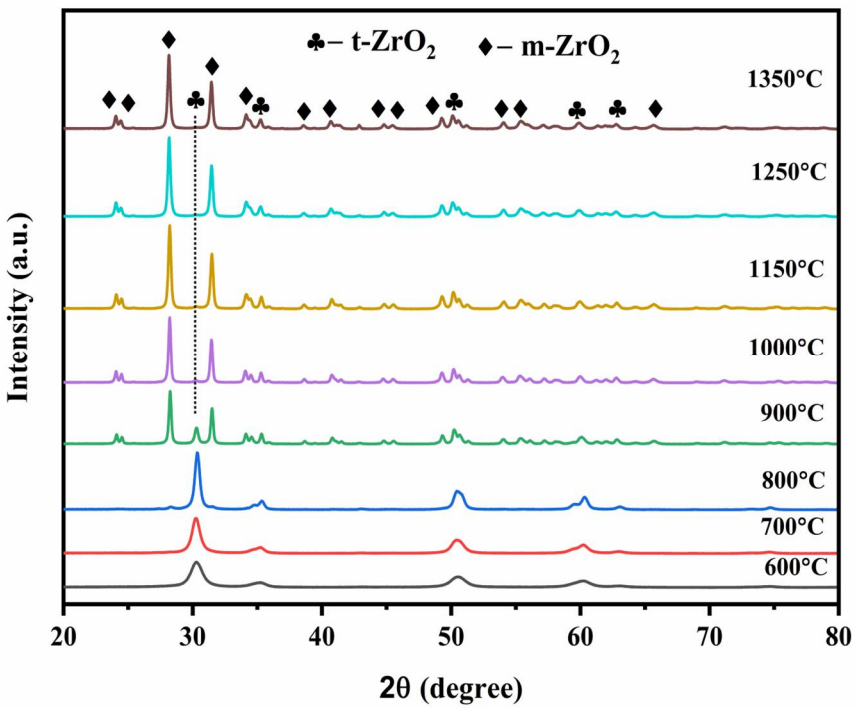

Fig. 5.2 XRD patterns of the 8Mg-PSZ powder at different calcination temperatures.

5.2.2 XRD and microstructural analysis of the sintered composites

The XRD patterns of composite material sintered at 1150°C, 1250°C, and 1350°C are represented in Fig. 5.3(a-c). The results indicate that BG addition (0 to 25wt %) into 8Mg-PSZ enhances the retention rate of the t-ZrO_2 phase (reference code: 98-009-6104) at 1150°C, as represented in Fig. 5.3(a). With enhancing the sintering temperature from 1150°C to 1250°C, the retention of the t-ZrO_2 phase is decreased, but the retention is slightly increased with the BG addition (10 to 25wt %), as shown in Fig. 5.3(b). With further enhancement in the sintering temperature from 1250°C to 1350°C, the retention rate of the t-ZrO_2 phase is increased along with enhancing the BG (0 to 25wt %), as observed in Fig. 5.3(c). Similar observations have also been reported by previous researchers (Vasanthavel *et al.*, 2016) (Del Monte *et al.*, 2000). The addition of SiO_2 (Del Monte *et al.*, 2000) and combined additions of $Ca^{2+,}$ $PO4^{-3,}$ and SiO_2 (Vasanthavel *et al.*, 2016) act as aging resistance, which restricts the transformation from t-ZrO_2 to m-ZrO_2 (reference code: 98-009-6104). Since $Ca^{2+,}$ $PO_4^{-3,}$ and

SiO_2 are the essential parts of 13-93 BG, these constituents are raised by raising the quantity of 13-93 BG in 8Mg-PSZ ceramics. The XRD pattern (in Fig.5.3(d)) of the composite sample with a higher amount of BG (25 wt%) demonstrates some crystalline phases like t-ZrO_2 and m-ZrO_2. In addition to t-ZrO_2 and m-ZrO_2 crystalline phases, there are some additional crystalline phases are found in the form of $CaMgO_6Si_2$ (Diopside) (reference code: 98-011-1641), and $Ca_3O_9Si_2Zr$ (Baghdadite) (reference code: 98-003-3844), when composite materials are sintered at 1150°C, 1250°C, and 1350°C, as shown in Fig. 5.3(a-c). These crystalline phases are used in bone tissue engineering. Overall, the results indicate that the sintering temperature and addition of 13-93 BG both play an important role in phase transformation from t-ZrO_2 to m-ZrO_2.

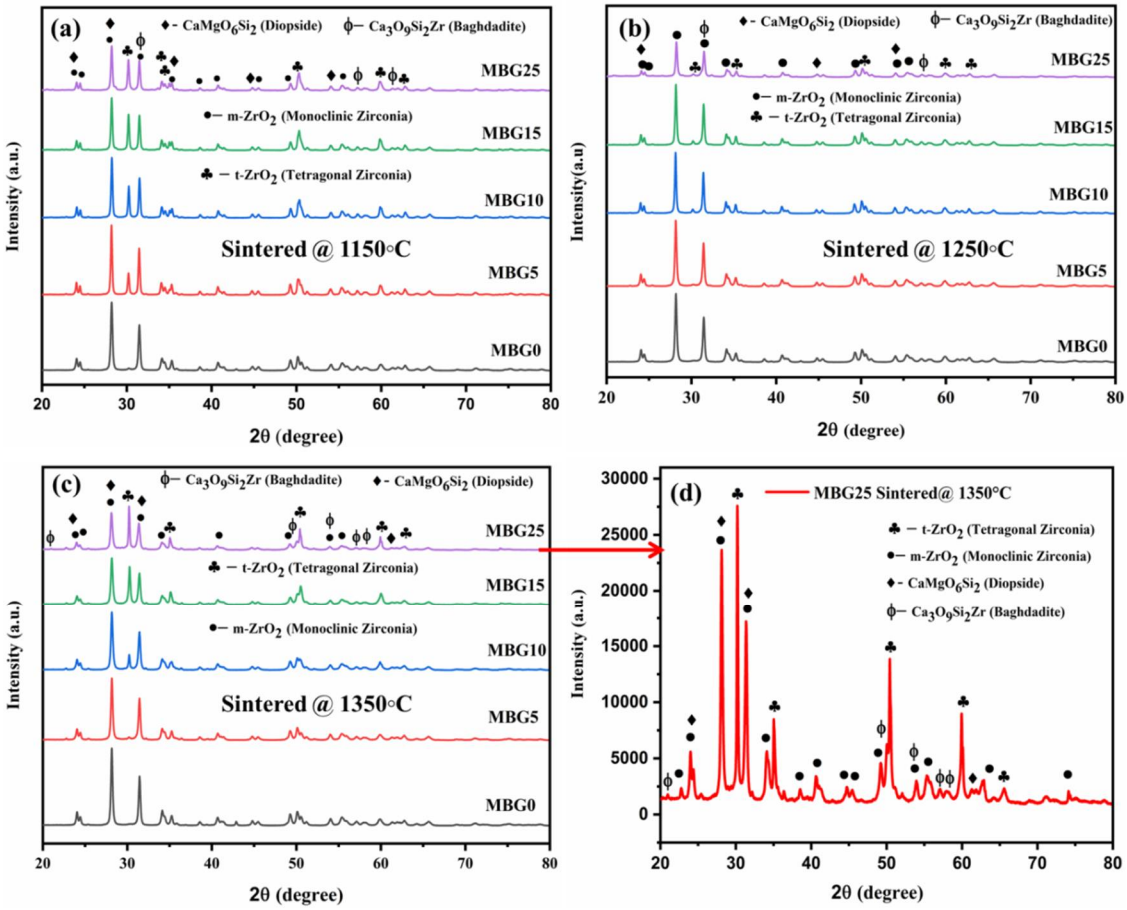

Fig. 5.3 (a-c) XRD patterns of the composite materials sintered at different temperatures, (d) XRD pattern of MBG25 composite at 1350°C.

SEM images of Mg-PSZ-based composite sintered at 1250°C and 1350°C with varying BG percentages (0%, 10%, and 25%) are represented in Fig. 5.4 & 5.5, respectively. It can be observed the loosening of the grains in Fig. 5.4(a), indicates that the Mg-PSZ has not been fully sintered at 1250°C. It has been proposed that Mg-PSZ should be sintered at a temperature of around 1550°C (Nawaz *et al.*, 2021).

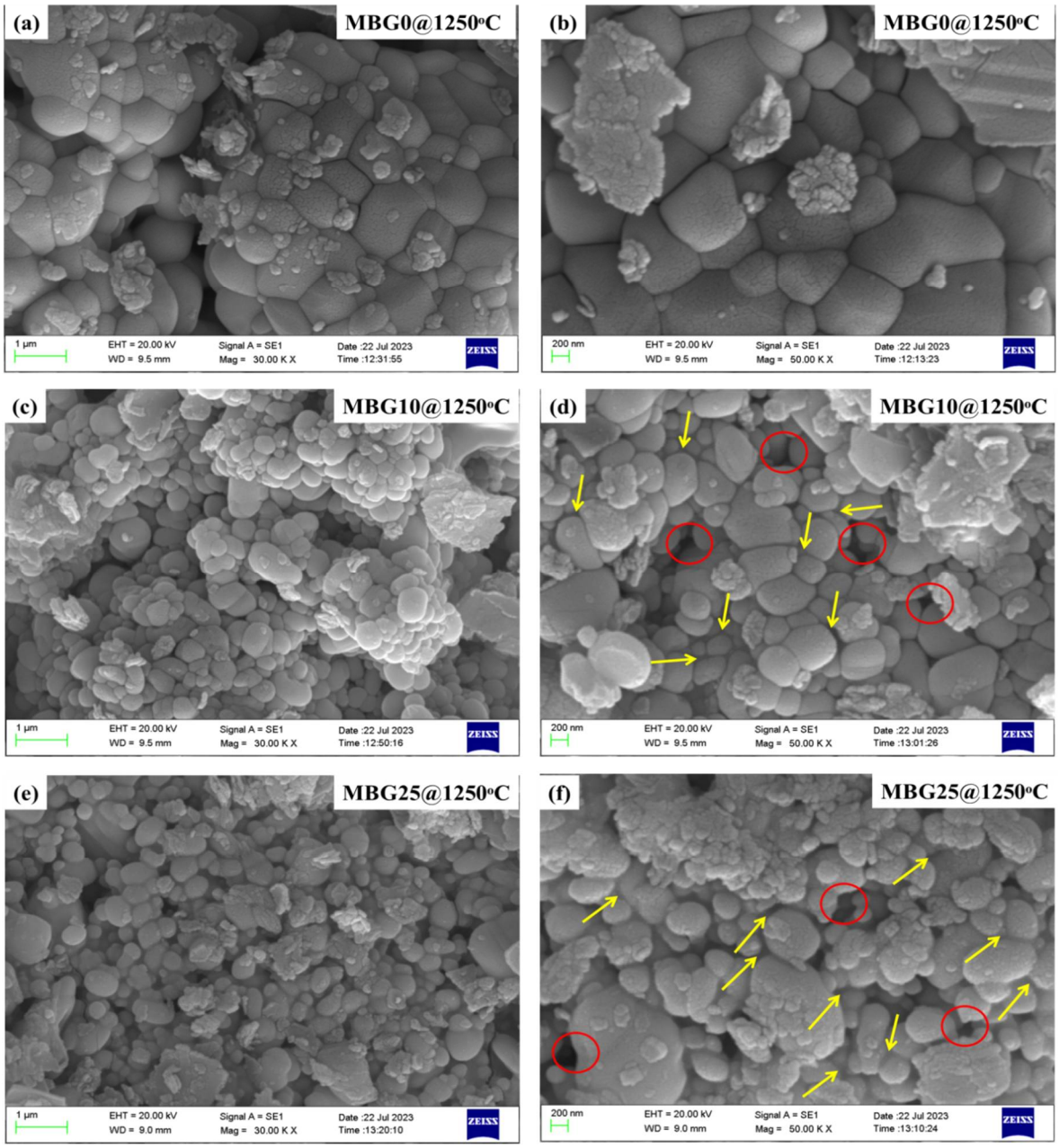

Fig. 5.4 (a-f) SEM images of 8Mg-PSZ-based bioceramic composite materials sintered at 1250°C temperature.

The specimen with 10% BG addition, as represented in Fig. 5.4(c & d), exhibits an improved sintering process. The BG particles considerably help the sintering process at 1250°C. The SEM image, shown in Fig. 5.4(e & f), indicates that the BG grains are partially incorporated into the crystalline grains. The intergranular spacing grows wider as the number of BG additions is increased. The crystalline grain is completely wetted with BG frits sintered at 1350°C, as shown in Fig. 5.5(c & d). With more glass additions, the intergranular gap is widened. The grain growth is obvious, and larger grain sizes are associated with higher sintering temperatures. The grain size of the sample with BG content of 25% is around 0.6 μm at 1250°C and 0.8 μm at 1350°C.

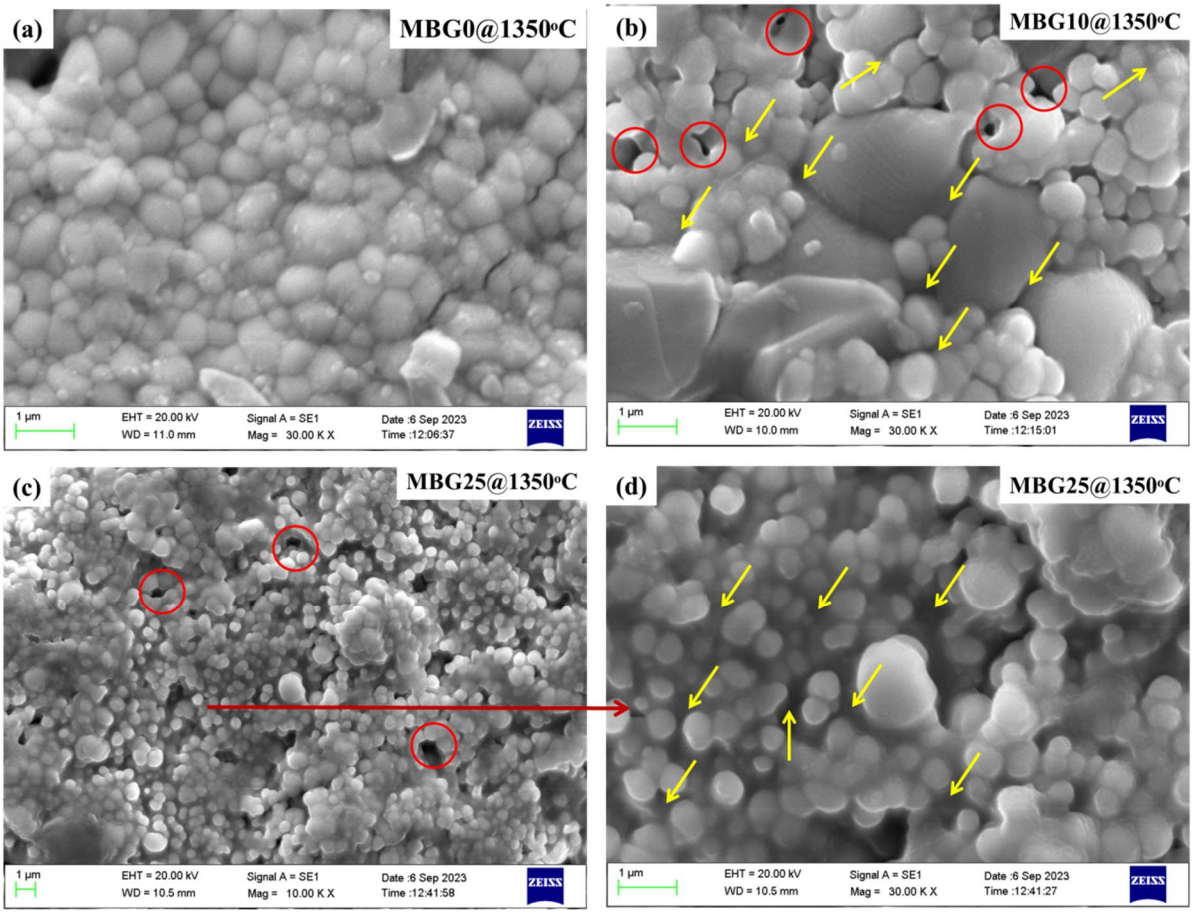

Fig. 5.5 (a-d) SEM images of 8Mg-PSZ-based bioceramic composite materials sintered at 1350°C temperature.

The SEM morphology analysis, as illustrated in Fig. 5.4 and Fig. 5.5, confirms the presence of a thin intergranular glassy phase (indicated by yellow arrows) along the grain boundaries within the surface layers of Mg-PSZ-based BG composite samples.

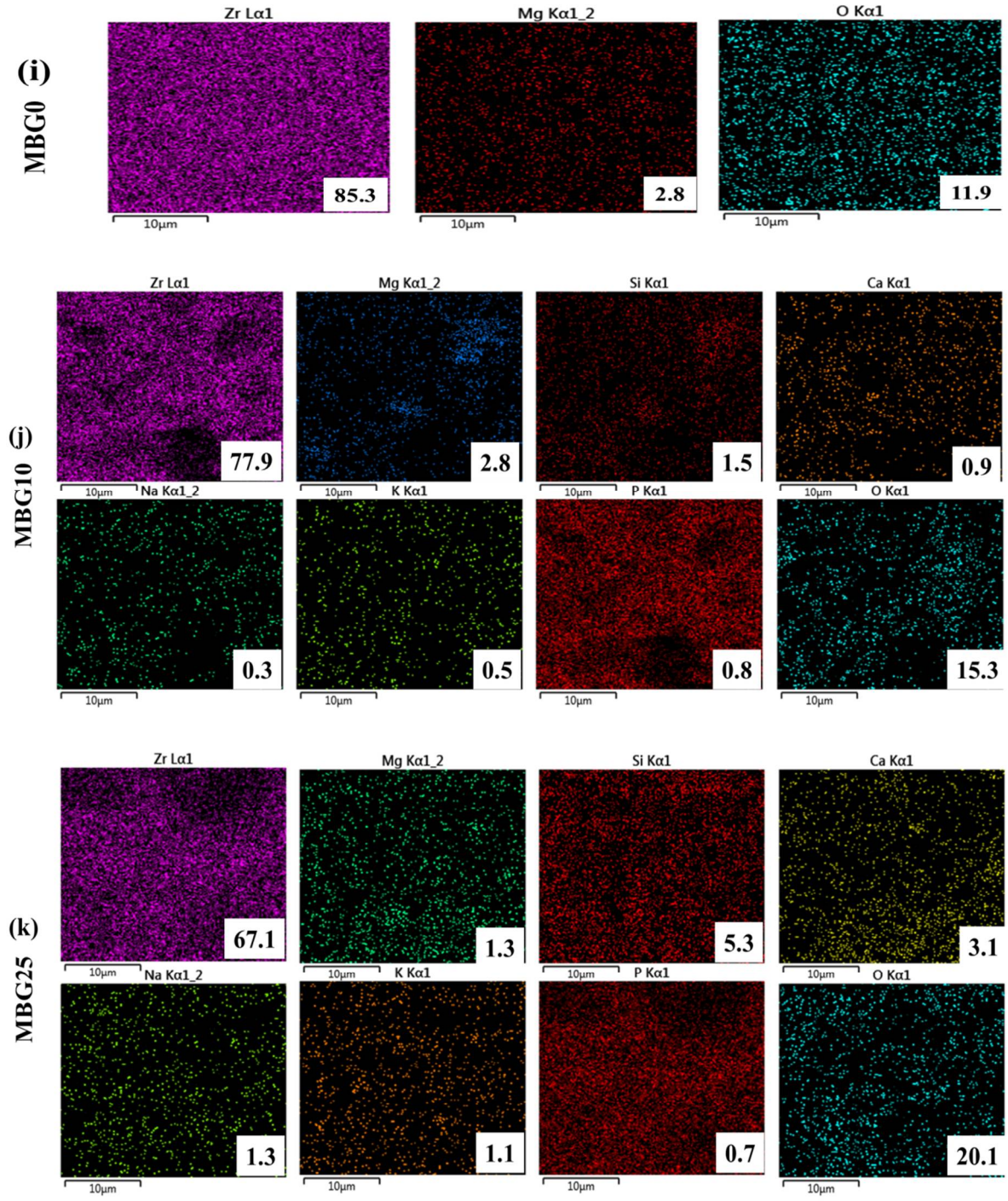

Fig. 5.6 (i-k) Elemental mapping of bioceramic composite with different BG content (0%, 10%, and 25%) at 1350^{o}C.

Both the grain boundaries and pores (indicated by red circles) are filled with a considerable amount of the glassy phase. The intergranular phases originating from the BG demonstrate a seamless integration with the Mg-PSZ grains. Notably, there is no apparent distinction between the glassy phase and the Mg-PSZ grains. Consequently, a strong bond between BG and Mg-PSZ is expected, mitigating the risk of inadequate adhesion strength associated with the use of bioactive glass infiltration into the Mg-PSZ matrix to enhance tissue integration.

Fig. 5.6(i)–(k) displays the EDS mapping of bioceramic composite with different BG content (0%, 10%, and 25%) at 1350ºC. Several elements, including Zr, Si, Ca, Na, Mg, K, P, and O, are present in the composite samples due to BG content. Additionally, it guarantees a uniform distribution of all the components without the addition of unnecessary impurities. The results show that as the BG concentration increases, the weight percentage of the Zr element decreases. The mechanical properties of Mg-PSZ are really determined by the percentage of the preserved t-phase at room temperature, which relies on the grain size and MgO concentration in the ceramics (Rahaman *et al.*, 2008).

5.2.3 Measurement of density and mechanical properties

Table 5.1 displays the sintered specimens' experimental, theoretical, and relative densities as a function of sintering temperature and BG concentration. The theoretical density values, 6 g/cm^3 for Mg-PSZ and 2.70 g/cm^3 for 13-93 bioactive glass are used to calculate the relative densities. The relative density first decreases as the BG concentration is increased up to 10 wt%, then marginally enhances up to 25 wt% of BG addition at 1250°C sintering temperature. The experimental density is lower due to the intergranular glassy phase. But, the relative density decreases with BG concentration up to 15 wt% at 1350ºC. Specimens sintered at 1350°C present better densification compared to 1250°C. The improved

densification of biocomposite materials with temperature is due to the addition of BG frits, which wet the crystalline grain and accelerate densification. Particles bond easily when the sintering temperature rises because the liquid's viscosity is lowered (Vasanthavel *et al.*, 2016).

Table 5.1 Theoretical density along with experimental density, relative density, and percentage porosity of sintered composite at different temperatures.

S. No.	Sample Code	Theoretical density (gm/cc)	Sintered at 1250°C			Sintered at 1350°C		
			Experimental density (gm/cc)	Relative density (%)	Porosity (%)	Experimental density (gm/cc)	Relative density (%)	Porosity (%)
1.	MBG0	6.0	5.48±0.06	91.33±0. 9	8.66	5.64±0.07	94.00±0.7	6.00
2.	MBG5	5.65	5.13±0.05	90.79±1.1	9.21	5.22±0.08	92.33±0.8	7.67
3.	MBG10	5.34	4.58±0.09	85.76±0.8	14.24	4.94±0.07	92.50±1.1	7.50
4.	MBG15	5.07	4.44±0.07	87.57±0.9	12.43	4.55±0.09	89.74±0.7	10.26
5.	MBG25	4.59	4.05±0.07	88.23±1.1	11.77	4.28±0.09	93.24±0.9	6.76

Table 5.2 Mechanical properties of Mg-PSZ-based composite materials sintered at different temperatures.

S. No.	Sample Code	Sintered at 1250°C			Sintered at 1350°C		
		Flexural strength (MPa)	Compressive strength (MPa)	Hardness (GPa)	Flexural strength (MPa)	Compressive strength (MPa)	Hardness (GPa)
1.	MBG0	310±28	425±34	2.47±0.8	560±35	820±54	3.44±0.9
2.	MBG5	325±36	442±41	2.77±0.9	545±47	788±59	4.07±0.8
3.	MBG10	348±29	460±45	2.87±0.7	510±37	753±52	4.79±0.9
4.	MBG15	372±39	490±39	3.34±0.4	475±32	732±43	6.19±1.0
5.	MBG25	420±32	530±46	3.87±1.0	496±41	750±47	6.79±1.3

Table 5.2 shows the flexural strength, compressive strength, and hardness of Mg-PSZ-based composites as a function of the sintering temperature and BG addition. When the sintering temperature is increased from 1250°C to 1350°C, the flexural strength, compressive strength, and hardness are increased in comparison to composite sintered at 1250°C. This enhancement is due to better densification (Vasanthavel *et al.*, 2016) (Del Monte *et al.*, 2000). Because the viscosity of BG is reduced when the sintering temperature is increased from 1250°C to 1350°C, and it can easily enter into the gaps between the grains and wet the matrix particles, as represented in Fig. 5.5(b, c, and d). The infiltration of BG into the Mg-PSZ can fill the void and compact the samples, as shown in Fig. 5.5(b, & c). Further, the flexural strength, compressive strength, and hardness are increased by enhancing the BG (0 to 25 wt %) sintered at a low temperature of 1250°C. Since 8Mg-PSZ requires a high sintering temperature of about 1550°C for sufficient densification (Nawaz *et al.*, 2021) at 1250°C, samples are not completely sintered, but it is observed that the addition of BG particles into 8Mg-PSZ, enhances the mechanical properties. This enhancement is due to BG frits, which are wetted the 8Mg-PSZ particles and compacted at 1250°C. Further, at a higher sintering temperature of 1350°C, hardness is enhanced by increasing the BG content (0 to 25 wt %), while flexural strength and compressive strength are decreased by enhancing the BG content up to 15 wt.% afterward slightly enhanced up to 25 wt%. Similar observations are also found in the case of elastic modulus measurement.

Table 5.3 represents the elastic modulus such as L_m, E, G, K, and σ of Mg-PSZ-based composite sintered at 1350^{o}C. Elastic modulus such as E, G, and K are decreased up to 15 wt% of BG addition and then slightly increased up to 25 wt% BG addition. The Poisson's ratio (σ) is highest (0.35) for the Mg-PSZ sample and lowest (0.21) for the sample containing 25 wt% of BG. Such trends occur due to the fact that BG additions reduce the mechanical characteristics of the samples. In the composite sample containing a higher BG amount (25

wt%), the intergranular space may be widened, and the BG frits are easily infiltrated by wetting the matrix particles, as observed in SEM Fig. 5.5(b, c, & d).

Table 5.3 Elastic modulus of Mg-PSZ-based composite material sintered at 1350°C.

S. No.	Sample Code	V_L (m/s)	V_T (m/s)	L_m (GPa)	E (GPa)	G (GPa)	K (GPa)	σ
1.	MBG0	5112	2472	147.39	92.86	34.46	101.44	0.35
2.	MBG5	4786	2498	119.56	85.51	32.57	76.13	0.31
3.	MBG10	4473	2519	98.84	79.46	31.34	57.05	0.27
4.	MBG15	4498	2584	92.05	76.17	30.38	51.05	0.25
5.	MBG25	4717	2868	95.23	84.95	35.20	49.29	0.21

Consequently, the mechanical properties are slightly improved by increasing densification and compacted structure. Overall, two noteworthy impacts related to the presence of BG reinforcements are indicated by the mechanical property results. The mechanical characteristics are increased when BG reinforcements are present during the lower sintering temperatures, and they decline when BG additives are present during higher sintering temperatures. *Cuy et al.* have stated that the maximum hardness (3.5 GPa) of teeth enamel is located on the surface, and the hardness decreases gradually with increasing depth (Cortés *et al.*, 2006). E_Mahoney *et al.* have observed that the elastic modulus for the enamel of teeth is 80.35±7.71 GPa (Mahoney *et al.*, 2000). In the present study, the biocomposite shows the hardness and elastic modulus values within the same range. The result indicates that the present composite may be used as enamel material for teeth with enhanced biological properties. The 8Mg-PSZ-based biocomposite with low bioglass content also shows very low hardness values. Pure bioactive glass is not used as a bone graft material due to its brittleness nature and low fracture resistance. For bone grafting, the properties required for the materials are low hardness, biocompatibility, structural integrity, adequate porosity, and compressive

strength. The choice of materials for bone grafts is crucial to ensure successful integration and healing. Bone graft materials should ideally have hardness similar to that of the surrounding bone to avoid stress shielding, which can lead to bone resorption. This helps in maintaining a more natural biomechanical environment for the bone. The 8Mg-PSZ-based biocomposite may be explored in bone grafting applications. The 8Mg-PSZ-based biocomposite can also be engineered into scaffolds with low hardness to mimic the mechanical properties of natural bone.

5.2.4 Biodegradation and bioactivity study

5.2.4.1 pH analysis

The changes in pH value of the bioceramic composite made of 8Mg-PSZ and 13-93 BG over the course of 35 days of dipping in the SBF are depicted in Fig. 5.7(a). The beginning pH of SBF is maintained at 7.40 for all samples. The pH-rising trend for all composite samples up to 14 days is caused by the interactions of ions, such as Na^{+}, Ca^{+}, K^{+}, etc., in the samples with cations of SBF (H^{+} or H_3O^{+}). It produces a negatively charged surface that draws Ca^{+2} ions existing in SBF (Mohammadi *et al.*, 2021). The phosphate and calcium in the sample induce the surface to form an apatite layer and lower the pH (Fathi *et al.*, 2007) (Li *et al.*, 2005). As immersion duration is prolonged, the pH of SBF almost remains constant for all samples. The deposition of the hydroxyapatite layer is validated by XRD, FTIR, and SEM with EDS analyses.

5.2.4.2 Biodegradation analysis

The right concentration of $Ca^{2+,}$ $P^{5+,}$ and Si^{4+} ions is crucial for osteogenesis; hence, bio-degradation is a crucial criterion for synthesized biomedical materials (Hoppe *et al.*, 2003). In SBF solution media, silicate-based biomaterials typically degenerate by dissolving

(Vyas *et al.*, 2015). In the current investigation, the integration of 13-93 BG is chosen to control the rate of decomposition of 8Mg-PSZ bio-ceramics, as represented in Fig. 5.7(b). The results show that the % W_L grows as immersion duration in SBF increases, and it then follows an almost constant pattern. It can result from an interaction of ions between the substance and the SBF solution (Zhang *et al.*, 2022). It also rises as the amount of BG inclusion is increased. This may be due to the drop in the experimental density with BG content. The decreased densification encourages biodegradation. Faster dissolving is achieved by high porosity and encourages ionic contact between the bioceramic and its surrounding SBF solution (Devi *et al.*, 2017) (Sarkar *et al.*, 2019).

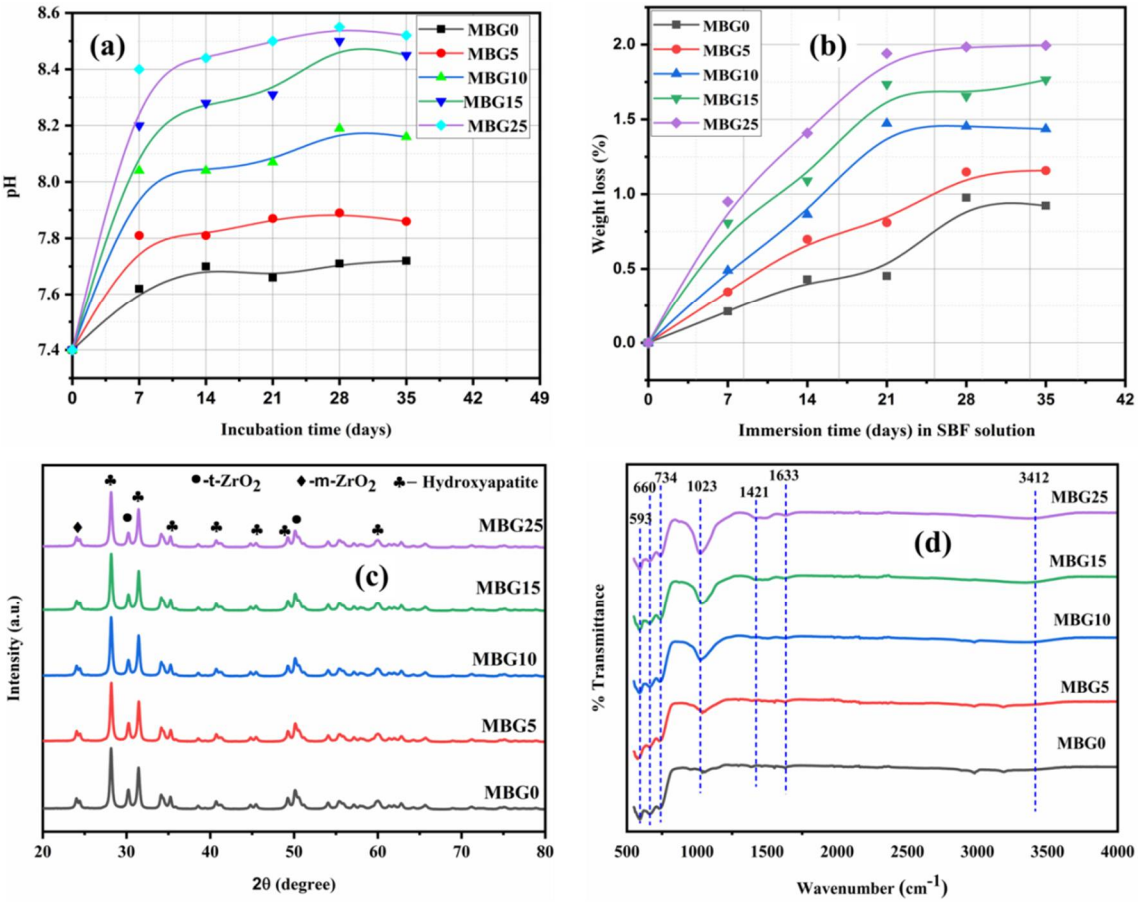

Fig. 5.7 (a) pH measurement with different time intervals, (b) *In-vitro* biodegradability analysis, (c) XRD patterns after 35 days of immersion in SBF, (d) FTIR spectra after 35 days of immersion in SBF.

5.2.4.3 Bioactivity analysis

After 35 days of submersion in SBF solution, all samples' surface morphology and EDS mapping are analyzed, as represented in Fig. 5.8(a-c). The surface of the 8Mg-PSZ ceramic substrate shows little evidence of apatite enrichment, as shown in Fig. 5.8(a), while *in-vitro* bioactivity studies clearly reveal the significant mineralization ability of the 8Mg-PSZ/13-93 BG composite, as shown in Fig. 5.8(a-c). After immersing all samples in SBF, a new layer developed with the typical flake look of apatite. According to the morphology of all samples, adding more BG to 8Mg-PSZ ceramic increases the ability of the apatite to mineralize. Additionally, EDS mapping of the composite samples makes clear the presence of Ca, P, and O, which are vital components of HA, whereas only Zr, Mg, and O are identified in the EDS mapping of the base 8Mg-PSZ ceramic. The layer may be apatite that lacks calcium, according to the Ca to P atomic ratio detected by EDS. XRD also supports the emergence of an apatite film on the top layer of the composite samples made up of 8Mg-PSZ and 13-93 BG, as shown in Fig. 5.7(c). The crystalline phase of HA (Reference Code: 98-006-0211) is identified in this structure after 35 days of submersion, according to the XRD results of all samples. FTIR analysis confirms the development of HA on the submerged outermost layer of all samples, as shown in Fig. 5.7(d). After 35 days of incubation period in SBF, the FTIR spectra indicate that all composite samples show apatite layer formation, which is validated by XRD, although there was no significant change in transmittance spectra of base 8Mg-PSZ ceramic following immersion in SBF. In FTIR spectra, transmittance bands appeared at 593, 660, 734, 1023, 1421, 1633, and 3412 wavenumbers (cm^{-1}). The bands at 500-660 and 1023 cm^{-1} are attributed to phosphate bands (PO_4^{-3}) (Rameshbabu *et al.*, 2005). The transmittance bands at 1421 cm^{-1} of the samples submerged in SBF show the presence of carbonate ions in the sample. The band at 1633 cm^{-1} is associated with C–O (stretch) and C=O (stretch) stretching modes (Vyas *et al.*, 2015). The chemical reaction between carbon dioxide

and a solution with a high pH could produce the carbonate ion (Rameshbabu *et al.*, 2005). At 3412 cm^{-1}, an OH^- band is made (Rameshbabu *et al.*, 2005). With increasing BG quantity, the intensity of the characteristic band at 1055 cm^{-1} grows, indicating the development of greater HA crystallinity (Rameshbabu *et al.*, 2005). Variations in band intensity in SBF demonstrate apatite formation and decomposition (Rameshbabu *et al.*, 2005). It is obvious that as the BG content increases, the ions emitted from the sample's surface exchange with the SBF solution (Hoppe *et al.*, 2011). As a consequence, the conditions causing HA deposits became more frequent. No substantial HA band is observed for MBG0, which may be a result of the deposition layer being too thin to be seen. The surface-level HA formation of the 8Mg-PSZ/13-93 BG samples may follow a similar pattern to that of a typical BG system, where the surface-formed hydrated silica (Si-OH) acts as the main location for apatite nucleation. This process is followed by the disintegration of surface-bound Ca^{2+} ions and the anionic exchange of PO_4^{3-} from SBF, which leads to the formation of an HCA layer (Zhang *et al.*, 2022). More BG particles enter into 8Mg-PSZ as the BG addition increases, enhancing the dispersion of Si and Ca ions and accelerating the deposition of HA (Zhang *et al.*, 2022). The development of apatite on the 8Mg-PSZ/BG samples requires a longer time than it happens on the samples of pure BG because of the reduced bioactivity of BG after sintering at high temperatures (Zhang *et al.*, 2022). Initially, Si-O-Zr bonds may form at high temperatures, inhibiting the synthesis of Si-OH groups. The decrease in the amount of Si-O-Si bonds has a negative impact on the early stages of the formation of Si-OH, which act as the locations for apatite nucleation (Zhang *et al.*, 2022).

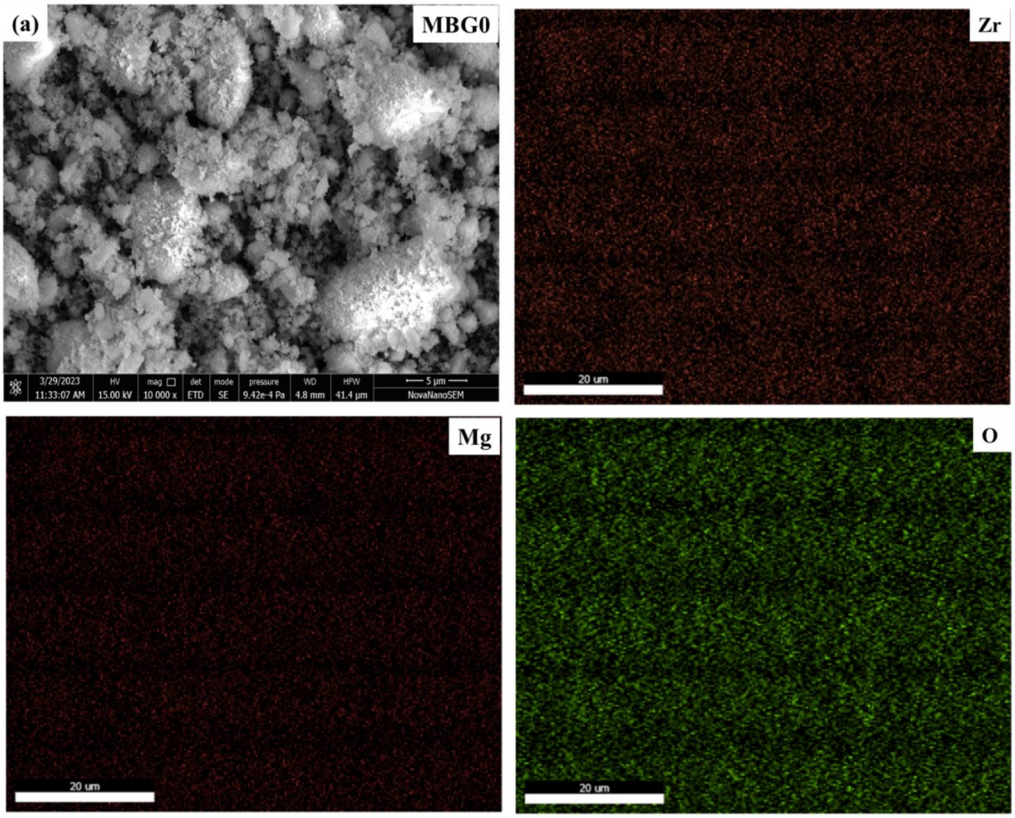

Fig. 5.8 (a) HR-SEM with elemental mapping of MBG0 sample after 35 days of immersion.

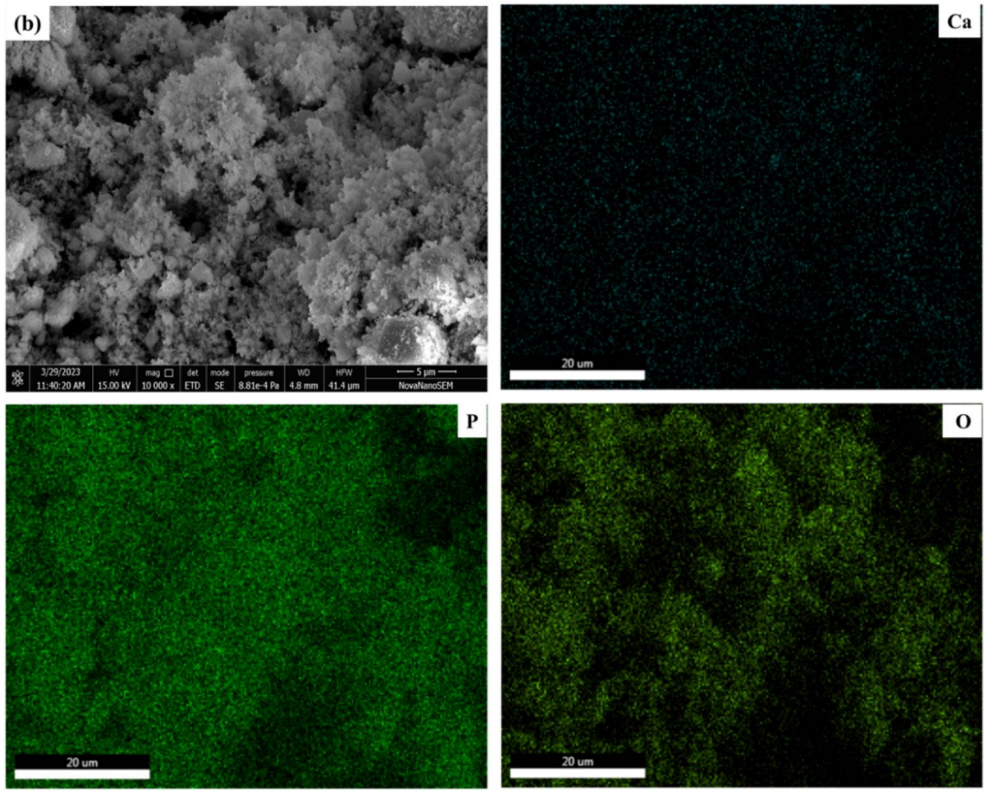

Fig. 5.8 (b) HR-SEM with elemental mapping of MBG10 sample after 35 days of immersion.

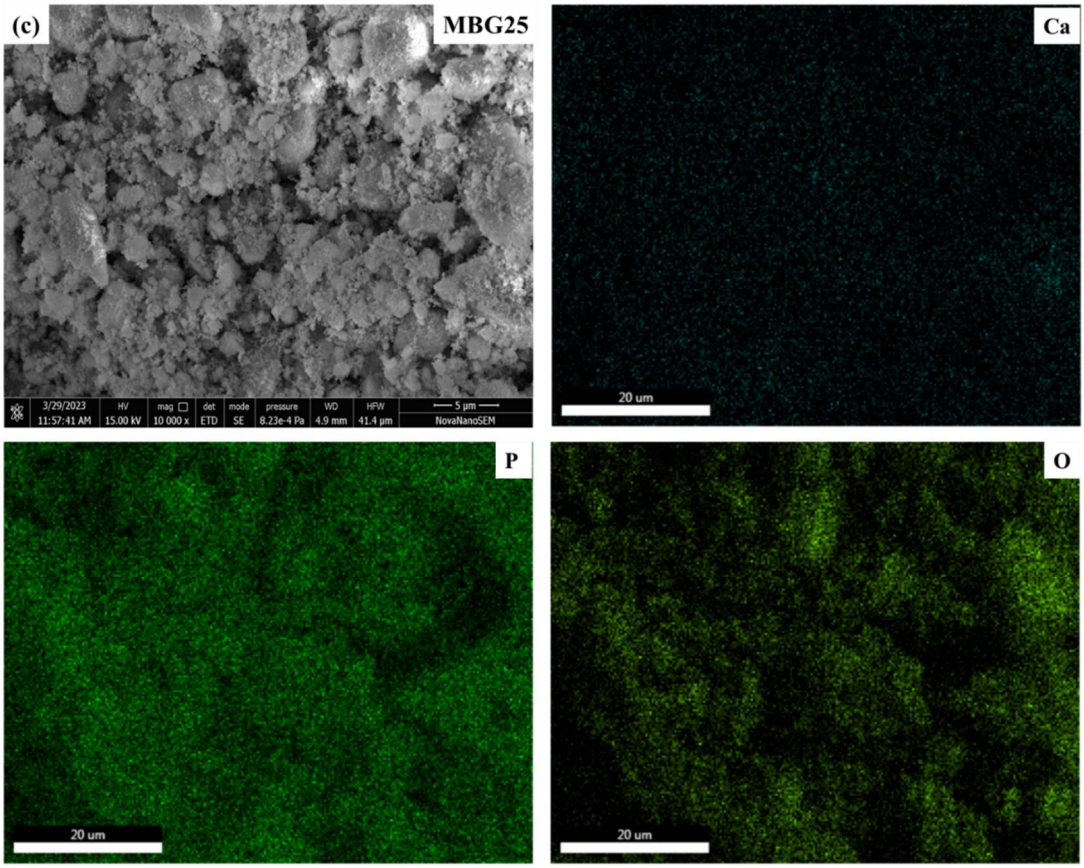

Fig. 5.8 (c) HR SEM with elemental mapping of MBG25 sample after 35 days of immersion.

5.2.4.4 Cell Culture Study

5.2.4.4.1 MTT assay result

Fig. 5.9 shows the viability of MG-63 cells in terms of cell proliferation after 3, 5, and 7 days of incubation. The cell viability of all the compositions (MBG0, MBG5, MBG10, MBG15, and MBG25) increases with enhancing culture times. It has been observed that the surfaces of 8Mg-PSZ/13-93 BG composites show excellent cell viability in comparison to pure 8Mg-PSZ samples after 3, 5, and 7 days. The cell viability of MG-63 cells on the surfaces of MBG5, MBG10, MBG15, and MBG25 samples is around 113, 125, 126, and 128%, respectively, after 3 days of incubation. However, after 5 and 7 days of incubation, the viabilities are improved by 104, 110, 123, and 131 % and 118, 120, 130, and 130 %, respectively, in comparison to the MBG0 sample. Except for the pure MBG0 sample, all of

the composite samples' optical densities show a considerable improvement over the control sample after 3, 5, and 7 days of incubation [represent as (*) in Fig. (5.9).

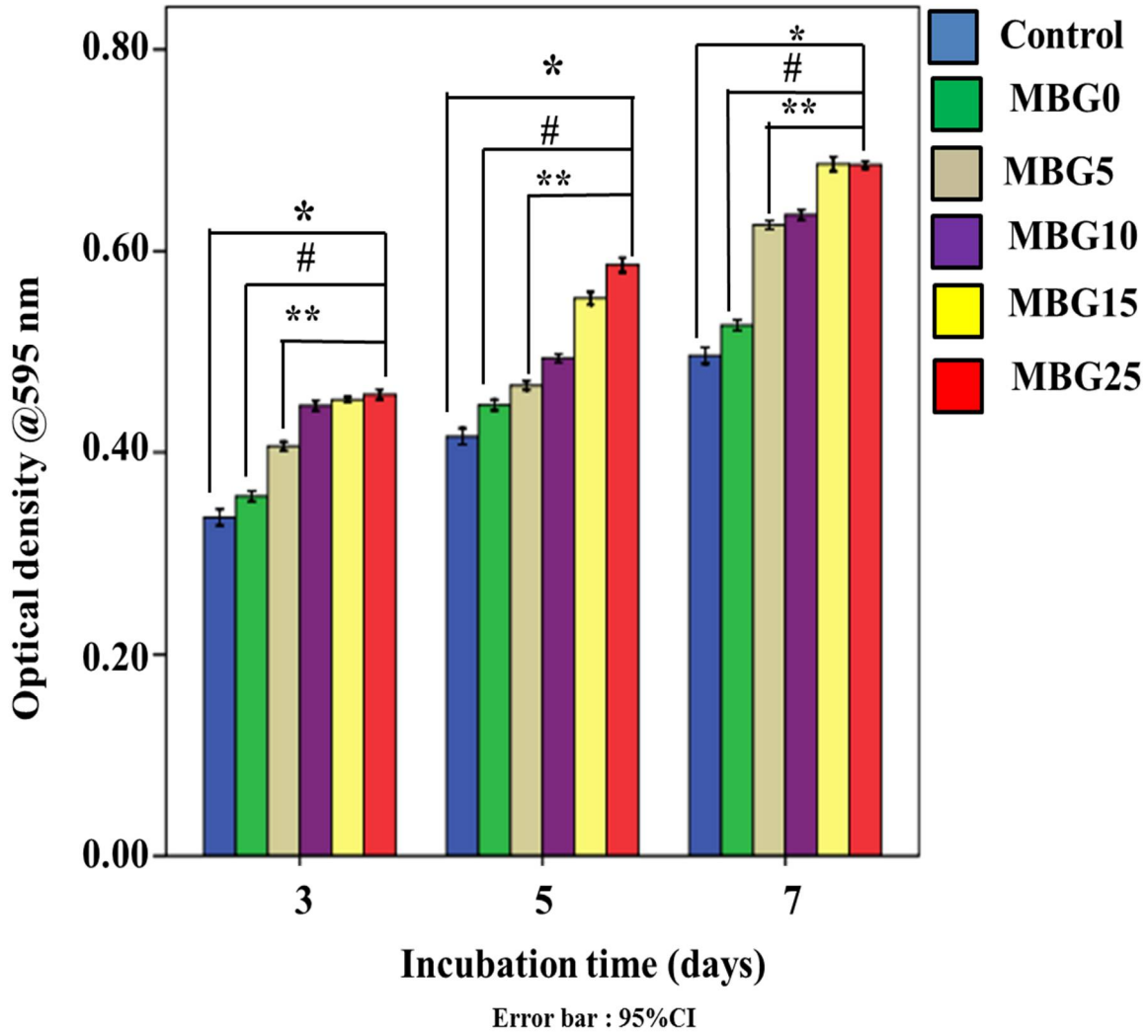

Fig. 5.9 MTT assay result for 8Mg-PSZ/13-93 BG bioceramic composite, cultured for 3, 5 and 7 days. The symbol **'*'** represents the statistically significant difference in the mean optical density for all samples in comparison to the control sample, **'#'** represents the statistically significant difference in the mean optical density for all bio-composite samples in comparison to the base samples MBG0. **'**'** represents the statistically significant difference in the mean optical density for MBG10, MBG15, and MBG25 samples in comparison to the MBG5 sample.

The optical densities of MBG5, MBG10, MBG15, and MBG25 samples have significantly improved after 3, 5, and 7 days of incubation as compared to MBG0 sample [represent as (#) in Fig. (5.9)]. Furthermore, the optical densities of MBG10, MBG15, and MBG25 composite samples significant increase as compared to MBG5 sample after 3, 5, and 7 days of incubation [represent as (**) in Fig. (5.9)]. The outcomes indicate that the proliferation of MG-63 cells is improved with the addition of BG into 8Mg-PSZ ceramic which is also confirmed by fluorescence microscopy images, as represented in Fig. 5.10. In *in-vitro* cell culture, composite samples made of 8Mg-PSZ and 13-93BG, release Ca^{2+}, PO_4^{-3}, and Si^{4+} ions into the culture media, which causes the surface of the composite samples to become silicon-rich (Verma *et al.*, 2020). At the same time, a strong negative charge is developed, allowing the proteins in the culture medium to be absorbed and encouraging cell proliferation. In summary, it is clear that the inclusion of BG into pure 8Mg-PSZ can considerably enhance the cellular response of 8Mg-PSZ.

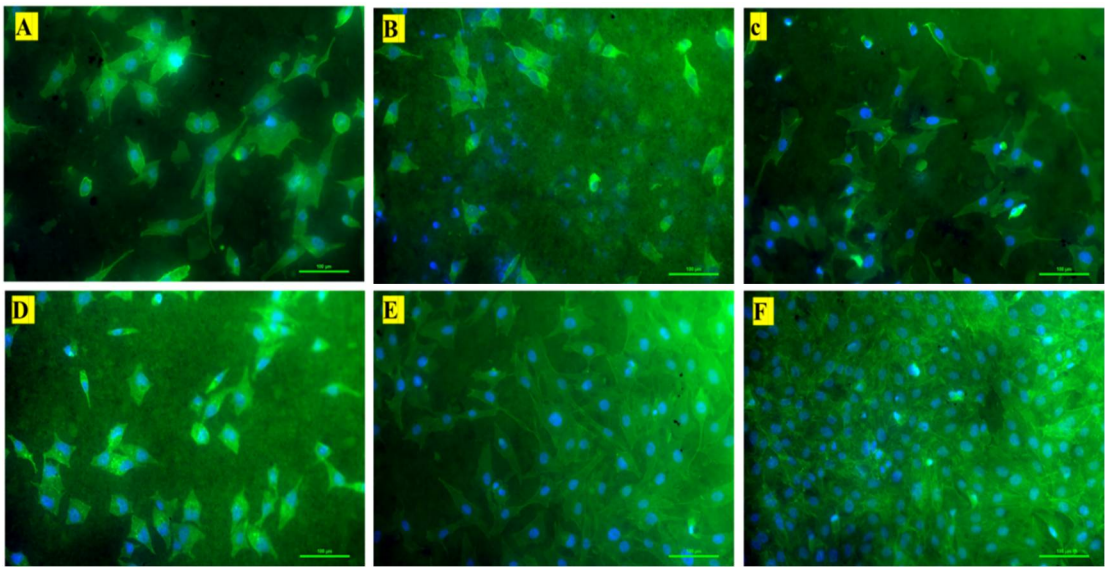

Fig. 5.10 Florescence microscopy images of MG-63 cells, adhered on the surface of 8Mg-PSZ/13-93 BG (0 to 25 wt% of BG) bioceramic composites cultured for 48 h, (A) Control, (B) MBG0, (C) MBG5, (D) MBG10, (E) MBG15, (F) MBG25. The scale bar represents 100 µm.

5.2.4.4.2 Fluorescence microscopy study

The adhesion of MG-63 cells on the pure 8Mg-PSZ and composite is examined under fluorescence microscopy, as represented in Fig. 5.10. Results show that the density of cells is improved on the surface of MBG5, MBG10, MBG15, and MBG25 samples as compared to the MBGO. In addition, the densities of MG- 63 cells on the surface of 8Mg-PSZ/13-93 BG composite are increased by enhancing the concentration of BG (0 to 25 wt%) into pure 8Mg-PSZ ceramic. Also, the adhesion of MG- 63 cells on the surface of the MBG0 sample appears to be higher and flattened as compared to the control. Additionally, compared to a pure MBG0 sample, the cells seem to be denser with increasing concentrations of BG in MBG5, MBG10, MBG15, and MBG25 samples. As a result, the MBG25 sample exhibits the highest cell density as compared to the pure MBG0 sample. The 8Mg-PSZ are reportedly bio-inert and do not support cellular functionality (Zhang *et al.*, 2022). Additionally, it has been found that adding BG to 8Mg-PSZ ceramics enhances the bioceramic composites' ability to promote cell growth (Ke *et al.*, 2017) (Silver *et al.*, 2001). Bioactive glasses emit ions that promote cell proliferation, osteoblast formation, and angiogenesis (Verma *et al.*, 2020). The biological and structure-related elements of bone growth and metabolism are known as osteoblasts (Valerio *et al.*, 2004). The alkaline character of the culture media is caused by the release of silicylic acid by BG due to ionic exchange (Xynos *et al.*, 2000) (Silver *et al.*, 2001) (Bosetti et al., 2003). However, such an occurrence may be detrimental to cells, and an increase in osteoblast viability and proliferation is seen. This is in accordance with a previous study where a link between alkalinization and the development of osteoblasts or chondroblasts occurred (Vrouwenvelder *et al.*, 1992). In addition, it is demonstrated that voltage-activated calcium channels are present in the cell membrane (Valerio *et al.*, 2004) (Khare *et al.*, 2022) (Singh *et al.*, 2023) and that alkalinization raises channel sensitivity, enabling cellular calcium entry (Rhee *et al.*, 2003) (Seaborn *et al.*, 2002). The present findings are in good

agreement with enhanced proliferation in the existence of ionic chemicals generated from BG in the media. Table 5.4 compares the results of the current research study on the biological properties of the present material with those of previously published research work.

5.2.4.5 Antibacterial analysis

Fig. 5.11 shows the variation in mean O.D. of 8Mg-PSZ and 8Mg-PSZ –xBG (x = 0, 5, 10, 15, and 25 wt%) composite systems against E. coli and S. aureus bacteria. The mean O.D. for both E. coli and S. aureus bacteria cells reduces with the addition of BG. Asterisks (@) and (#) represent the significant difference among all the samples with respect to control for E. coli and S. aureus bacteria, respectively [Fig. 5.11]. Asterisks (@) and (&) represent the significant difference among the composite samples (MBG5, MBG10, MBG15, and MBG25) with respect to the 8Mg-PSZ sample (MBG0) for E. coli and S. aureus bacteria respectively at $p \leq 0.05$ as shown in Fig. 5.11. 8Mg-PSZ–xBG composites decrease the mean O.D. significantly for S. aureus bacteria compared to 8Mg-PSZ [Fig. 5.11]. On the surfaces of MBG25, the density of S. aureus bacterial cells decreased by about 30%. The live/dead ratio of 8Mg-PSZ and 8Mg-PSZ –xBG (x = 0, 5, 10, 15, and 25 wt%) composite systems is calculated against E. coli and S. aureus bacteria with the help of O.D. of the samples. It is found that the live/dead ratio for E. coli and S. aureus bacterial cells decreases significantly with the addition of BG into 8Mg-PSZ. The live/dead ratio for E. aureus of MBG0, MBG5, MBG10, MBG15, and MBG25 are 13.99, 5.07, 3.32, 2.37, and 2.16, respectively. The live/dead ratio for S. aureus of MBG0, MBG5, MBG10, MBG15, and MBG25 are 15.42, 5.67, 3.74, 2.70, and 1.01, respectively. It can be observed from the antibacterial results that the BG (x = 0, 5, 10, 15, and 25 wt%) addition to 8Mg-PSZ enhances the antibacterial properties of 8Mg-PSZ. The antibacterial properties of BG are correlated with many parameters like changes in pH, dissolution rate, changes in concentration of alkali ions in

glass composition, and bacterial species (Zhang *et al.*, 2010) (Allan *et al.*, 2001) (Zehnder *et al.*, 2006).

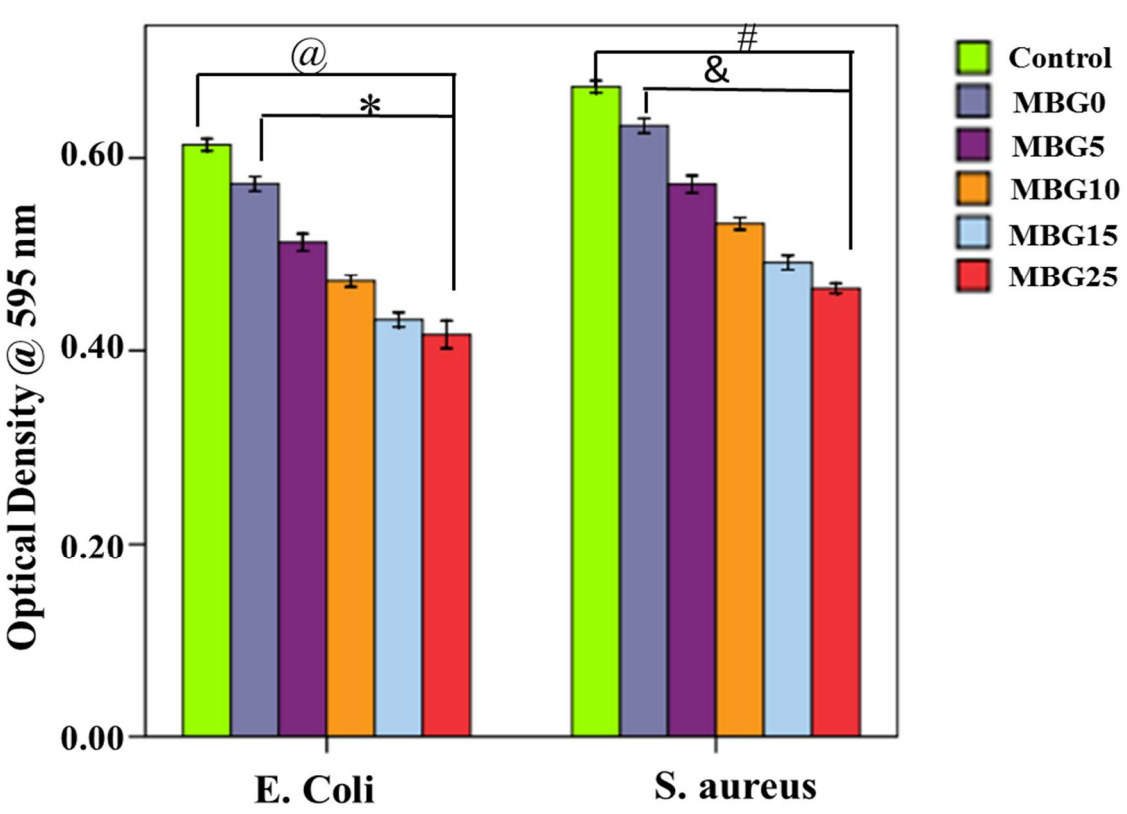

Fig. 5.11 Antibacterial response of 8Mg-PSZ and 8Mg-PSZ –xBG (x = 0, 5, 10, 15, and 25 wt%) composite for gram-negative (E. coli) and gram-positive (S. aureus) bacteria. Asterisks (@) and (#) represent the statistically significant difference among all the samples with respect to control for gram-negative (E. coli) and gram-positive (S. aureus) bacteria, respectively, at $p \leq 0.05$. Asterisks (*) and (&) represent the statistically significant difference among the composite samples (MBG5, MBG10, MBG15, and MBG25) with respect to the MBG sample (MBG0) for gram-negative (E. coli) and gram-positive (S. aureus) bacteria, respectively at $p \leq 0.05$.

Among them, antibacterial properties are affected by the increase in the pH inside the solution (Zhang *et al.*, 2010) (Allan *et al.*, 2001) (Zehnder *et al.*, 2006). Increasing glass dissolving tendency results in higher local pH and alkali ion concentrations in the solution,

improving the glass's overall antibacterial properties (Zhang *et al.*, 2010) (Allan *et al.*, 2001) (Zehnder *et al.*, 2006). In this study, *in-vitro* biomineralization results show that the pH and degradation rate of composite samples containing BG is increased with enhancing the BG concentration. This pH and degradation rate may help to improve the antibacterial properties of the 8Mg-PSZ –xBG composite. Another reason for improving antibacterial response is the presence of MgO in the BG composition. The MgO addition improves the antibacterial response of 8Mg-PSZ (Stoor *et al.*, 1998) (Taeh *et al.*, 2022).

5.3 Summary

In the current work, the structural, mechanical, and biological properties of the [(100-x) (8Mg-PSZ) – x (13-93 BG)] composite are examined. The relative density and mechanical characteristics show that both are significantly affected by the sintering temperature as well as BG content. The relative density and mechanical characteristics, such as flexural strength, compressive strength, and hardness are increased with the enhancement of the sintering temperature. The relative density of samples is almost decreased up to 10 wt% of BG, then slightly enhanced up to 25wt% of BG addition at both low and high sintering temperatures. The flexural strength, compressive strength, and hardness are improved at low sintering temperatures. At higher sintering temperatures, flexural strength and compressive strength are decreased up to 15 wt% of BG, and then it slightly increases up to 25 wt% of BG while hardness is increased with the BG additive up to 25 wt%. Elastic modulus decreases as BG content is added up to 15 wt%, and then it slightly increases up to 25 wt% at higher sintering temperature. The *in-vitro* bioactivity, biodegradability, cellular viability, and antibacterial response of the modified 8Mg-PSZ-based bioceramic composite materials are increased with increasing incorporation of 13-93 BG content.